machines

MDPI

Article

GES-YOLO: A Light-Weight and Efficient Method for Conveyor Belt Deviation Detection in Mining Environments

Hongwei Wang [1,2], Ziming Kou [1,2,*] and Yandong Wang [1,2]

[1] College of Mechanical Engineering, Taiyuan University of Technology, Taiyuan 030024, China; wanghongwei0086@link.tyut.edu.cn (H.W.); wangyandong@tyut.edu.cn (Y.W.)
[2] Shanxi Provincial Engineering Laboratory for Mine Fluid Control, Taiyuan 030024, China
* Correspondence: kouziming@tyut.edu.cn

Abstract: Conveyor belt deviation is one of the most common failures in belt conveyors. To address issues such as the high computational complexity, large number of parameters, long inference time, and difficulty in feature extraction of existing conveyor belt deviation detection models, we propose a GES-YOLO algorithm for detecting deviation in mining belt conveyors, based on an improved YOLOv8s model. The core of this algorithm is to enhance the model's ability to extract features in complex scenarios, thereby improving the detection efficiency. Specifically, to improve real-time detection capabilities, we introduce the Groupwise Separable Convolution (GSConv) module. Additionally, by analyzing scene features, we remove the large object detection layer, which enhances the detection speed while maintaining the feature extraction capability. Furthermore, to strengthen feature perception under low-light conditions, we introduce the Efficient Multi-Scale Attention Mechanism (EMA), allowing the model to obtain more robust features. Finally, to improve the detection capability for small objects such as conveyor rollers, we introduce the Scaled Intersection over Union (SIoU) loss function, enabling the algorithm to sensitively detect rollers and provide a precise localization for deviation detection. The experimental results show that the GES-YOLO significantly improves the detection performance in complex environments such as high-noise and low-illumination conditions in coal mines. Compared to the baseline YOLOv8s model, GES-YOLO's mAP@0.5 and mAP@0.5:0.95 increase by 1.5% and 2.3%, respectively, while the model's parameter count and computational complexity decrease by 38.2% and 10.5%, respectively. The Frames Per Second (FPS) of the average detection speed reaches 63.62. This demonstrates that GES-YOLO achieves a good balance between detection accuracy and inference speed, with excellent accuracy, robustness, and industrial application potential.

Keywords: belt conveyor; deviation detection; YOLOv8; light-weight network; deep learning

check for updates

Academic Editor: Antonios Gasteratos

Received: 13 January 2025
Revised: 5 February 2025
Accepted: 6 February 2025
Published: 8 February 2025

Citation: Wang, H.; Kou, Z.; Wang, Y. GES-YOLO: A Light-Weight and Efficient Method for Conveyor Belt Deviation Detection in Mining Environments. *Machines* **2025**, *13*, 126. https://doi.org/10.3390/machines13020126

Copyright: © 2025 by the authors. Licensee MDPI, Basel, Switzerland. This article is an open access article distributed under the terms and conditions of the Creative Commons Attribution (CC BY) license (https://creativecommons.org/licenses/by/4.0/).

1. Introduction

Being a key component of the coal transportation system, the belt conveyor plays an indispensable role in raw coal mining, conveying, and roadway excavation [1–3]. Conveyor belt deviation frequently occurs during prolonged operation under variable, uneven, and heavy loading conditions. If not detected and addressed promptly, deviation can worsen the edge wear on the belt, increase the running resistance, cause material spillage, and even lead to fire, halting underground production and transportation. This can result in significant economic losses and secondary accidents that threaten the safety of personnel [4,5]. Therefore, accurate detection of conveyor belt deviation and timely alarms are crucial to ensure the safe operation of coal mines and prevent serious accidents.

In the conveyor belt operation process, the phenomenon that the belt surface deviates from the original longitudinal centerline due to uneven force is called deviation. Statistics indicate that approximately 75% of belt conveyor accidents are caused by deviation. In the actual production of coal enterprises, design or manufacturing factors, installation quality factors and operational problems, and other factors can lead to conveyor belt deviation. But the ultimate reason is that in the process of movement force inequilibrium in the conveyor belt, force that is perpendicular to the direction of the belt speed of the horizontal velocity is formed, which results in conveyor belt deviation. As belt conveyors evolve toward higher speeds and longer distances, detecting deviation has become a major focus for researchers both domestically and internationally.

Currently, conveyor belt deviation detection primarily relies on manual, mechanical, or visual methods. Manual detection is labor-intensive, lacks real-time capability, and suffers from low efficiency and unreliable results [6,7]. Mechanical detection is based on the conveyor belt surface on both sides of the vertical roller device and the conveyor belt edge contact to determine whether runaway is occurring; often, because the material mistakenly touched something, which leads to false alarms, the precision is low [8]. Furthermore, the reliability of mechanical detection devices declines over time, increasing rather than decreasing operational risks. The widespread adoption of vision technology in the industrial sector has led to growing interest in machine-vision-based conveyor belt deviation detection methods.

Zhang et al. [9] proposed a conveyor belt deviation monitoring system that utilizes a camera and laser generator. The system employs edge detection and straight-line fitting techniques to extract the belt edges and determine the deviation status. Liu et al. [10] developed a template matching detection method based on the OM-SDD network, which employs Hough line transform to detect the edges of the conveyor belt and applies a geometric correction algorithm to estimate its deviation. While the above methods are capable of continuously detecting conveyor belt deviation, their recognition precision requires further improvement.

Yang et al. [11] designed an online monitoring system based on computer vision to address the issues of deviation and tearing in mining belt conveyors. They proposed a fast image segmentation method for real-time image processing, enabling the detection of longitudinal tearing and deviation in the conveyor belt. Zhang et al. [12] combined object detection networks to predict features and the conveyor belt's edge linear features, achieving quantitative monitoring of the conveyor belt deviation. All the above methods improve the detection efficiency, but the recognition precision is lacking in the poor-lighting environment underground.

Gao et al. [13] proposed a conveyor belt deviation detection method that combines deblurring and segmentation functions. This method utilizes object detection and semantic segmentation techniques to generate segmentation results for idler information and conveyor belt contours. By analyzing these results, the deviation of the conveyor belt is determined. Although this approach improves the recognition accuracy, it is cumbersome and slow, making it difficult to meet the demands of large-scale data detection. Zeng et al. [14] proposed a conveyor belt detection method based on a multi-scale feature fusion network to improve the detection efficiency, employing depthwise separable convolutions for real-time detection. The results show that the method achieves high detection accuracy with a detection rate of 13.4 FPS. However, it has not been tested on loaded conveyor belts, preventing validation of its practical performance.

Current research indicates that non-contact deviation detection methods using machine vision are gradually replacing other techniques due to their unique advantages [15–17]. However, the harsh operating conditions of underground belt conveyors in

coal mines limit the conventional detection devices' layout and diagnostic methods, which are insufficient to support real-time, comprehensive, and stable monitoring of conveyor belts. Therefore, developing a technology that is capable of real-time and accurate monitoring of conveyor belt operation and deviation warning in low-light, high-interference environments has become a crucial component in the intelligent development of coal mines.

Building on this, this paper proposes the GES-YOLO method for conveyor belt deviation detection, which is based on an enhanced YOLOv8s model. The key contributions of this paper can be summarized as follows: (1) To solve the problem of semantic information dropout during spatial compression and channel expansion in image data, we introduced Groupwise Separable Convolution (GSConv). GSConv maximizes the retention of hidden dependencies among channels, maintaining model precision while reducing computing complicacy. (2) To address the challenge of effectively extracting object features during sampling, the EMA attention mechanism is incorporated into the YOLOv8 backbone network, enhancing the feature extraction ability of GES-YOLO and improving its detection precision. (3) Through the dataset analysis, it was determined that an object detection layer that incorporates deeper semantic information is deemed unnecessary. Consequently, we removed the neck feature pyramid's deepest layer, together with the head's large object detection head, reducing both the parameter count and network depth, thus achieving a light-weight model. (4) Through ablation and performance comparison experiments, the effectiveness of the model in detecting conveyor belt deviation was thoroughly validated. The model achieved an mAP@0.5 of 98.74% and an mAP@0.5:0.95 of 87.53%, demonstrating optimal detection performance. Additionally, the model is only 13.3 MB in size, making it applicable for efficient deployment on edge devices.

The remainder of this paper adopts the following structure: Section 2 details the improvements that were made to the model. Section 3 reports experiments that were conducted on a self-constructed dataset, comparing the proposed method's performance with other classic algorithms. Finally, Section 4 presents the conclusion.

2. Improvement of YOLOv8s Deviation Detection Model for Mining Belt Conveyor

YOLOv8s, as a representative of the YOLO series, inherits and optimizes prior design principles, effectively extracting image features, achieving object detection, and maintaining high precision and speed [18]. However, the challenging environmental conditions in coal mine production demand higher speed, precision, and hardware efficiency for conveyor belt deviation detection [19]. To meet the detection requirements, this paper improves the original YOLOv8s network model and proposes a light-weight and efficient conveyor belt deviation detection method, named GES-YOLO. The overall structure of the GES-YOLO model is shown in Figure 1. In the backbone section, the two convolution (Conv) modules at the end are replaced with GSConv modules, and the EMA attention mechanism is added after the two Channel-to-Feature (C2f) modules at the end, aiming to improve the detection accuracy and reduce the computational complexity of the model. In the head section, the redundant 20×20 large object detection layer is removed, further reducing the number of model parameters. In the backbone section of Figure 1, Conv represents the standard convolution, GSConv denotes the light-weight convolution, and the C2f module is used for feature aggregation. Spatial Pyramid Pooling—Fast (SPPF) refers to the Spatial Pyramid Pooling module, which is responsible for fusing features at different scales. In the neck section, Upsample is the upsampling module, and Concat is the feature concatenation module. The head section includes detection heads for 80×80 and 40×40 objects.

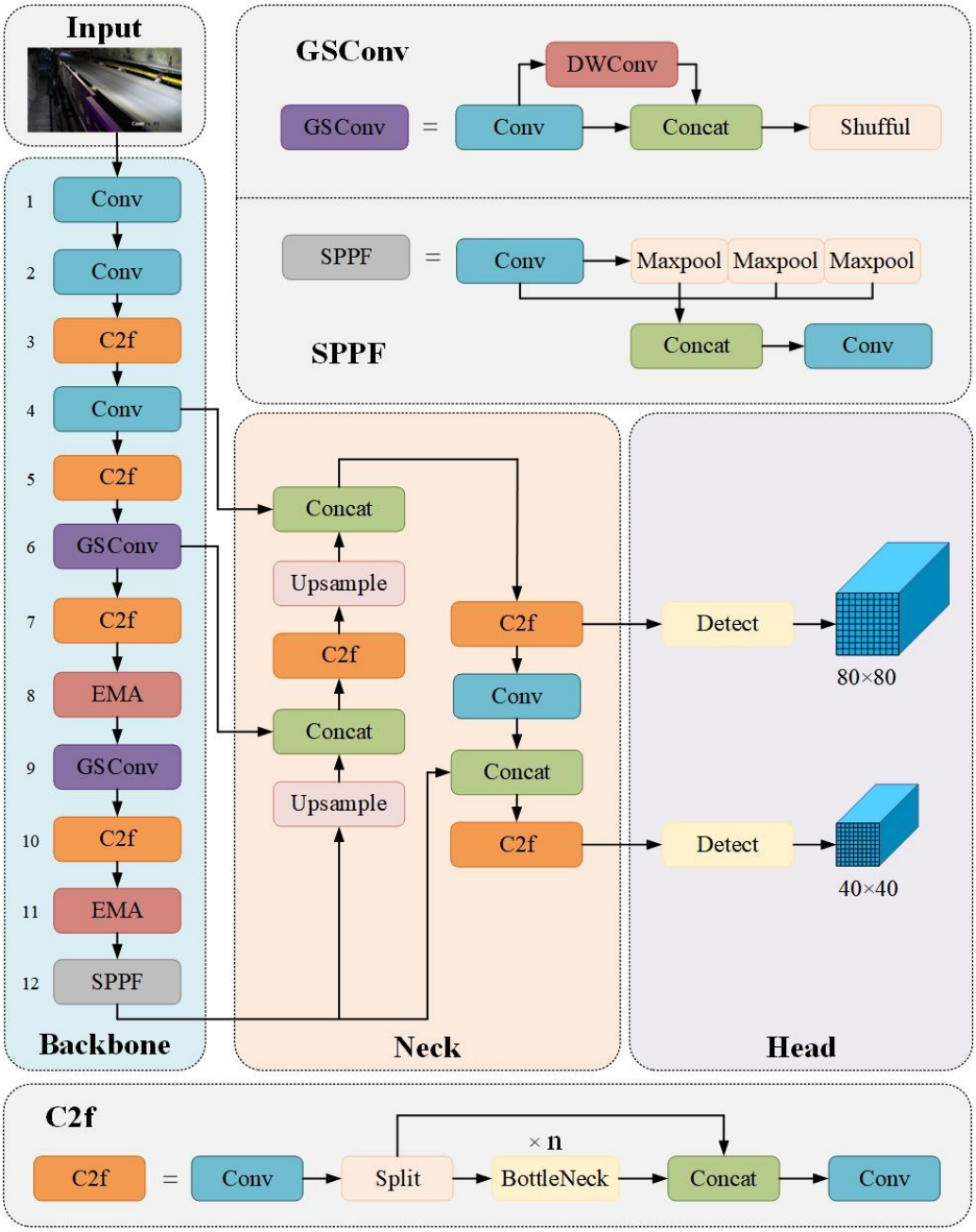


Figure 1. Structure of the improved YOLOv8s model (GES-YOLO).

2.1. Light-Weight Convolution Module, GSConv

YOLOv8 uses standard Conv to extract image features. However, excessive use of Conv results in a significant increment in computing complicacy and parameters, resulting in redundant features that impact the inference speed [20]. Since real-time detection is crucial for conveyor belt deviation detection, the model must be light-weight to meet this requirement. In practice, to improve object detection in dynamic environments and meet real-time requirements, the Conv standard convolution is often employed to replace depth-separable convolution (DSConv) [21]. However, DSConv causes some semantic information dropout during spatial compression and channel expansion, which negatively affects object feature extraction. To address the limitations of both standard Conv and DSConv, Li et al. [22] introduced the GSConv, a novel light-weight convolution module. Its main feature is the ability to minimize the computing complicacy while maintaining a high detection precision.

The GSConv convolution module operates by first performing downsampling using a standard convolution, followed by applying DWConv convolution. The outputs of these two convolutions are then combined. Next, the feature mappings are grouped along the channel dimension, with interleaving and rearrangement of the channels from both convolution outputs. Using a uniform mixing (Shuffle) operation, the information from the standard convolution is integrated with that of the depth-separable convolution [23]. This approach preserves channel interactions, minimizes time loss, enhances the feature diversity and richness, and reduces the computing complicacy. Please see Figure 2 for the GSConv module structure.

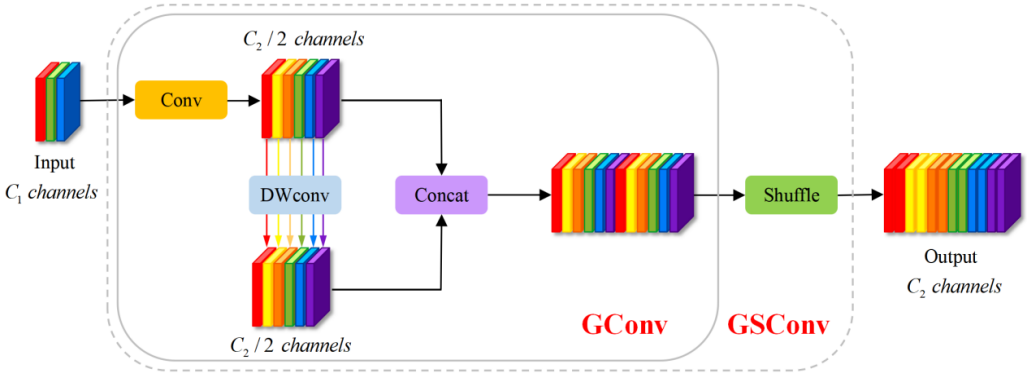


Figure 2. Structure of the GSConv module.

The computational parameter counts for Conv, DSConv, and GSConv are as follows:

$$Time_{Conv} \sim O(W \times H \times K_1 \times K_2 \times C_1 \times C_2) \tag{1}$$

$$Time_{DSConv} \sim O(W \times H \times K_1 \times K_2 \times 1 \times C_2) \tag{2}$$

$$Time_{GSConv} \sim O\left[W \times H \times K_1 \times K_2 \times \left(\frac{C_2}{2}\right) \times (C_1 + 1)\right] \tag{3}$$

where W stands for the output feature map width, H denotes the output feature map height, $K_1 \times K_2$ denotes the convolutional kernel size, C_1 denotes the channel number in each convolutional kernel, and C_2 denotes the channel number in the output feature mapping. DSConv shows the lowest time complexity when C_1 is greater than 1. GSConv is between Conv and DSConv, reducing the computational cost by approximately 50%. While Conv preserves hidden connections between channels, DSConv eliminates them entirely, significantly lowering the complexity. In contrast, GSConv retains these connections with a lower time complexity, thus reducing the computational cost while maintaining strong feature extraction capabilities [24].

2.2. Efficient Multi-Scale Attention Mechanism, EMA

During object detection in the complex underground environment of coal mines, problems such as severe occlusion, numerous interferences, and poor image quality make it difficult for the YOLOv8s network to effectively extract key features of the object during sampling. These challenges significantly increase the difficulty of detecting conveyor belt deviations. To solve this problem, we introduce the Efficient Multi-Scale Attention Mechanism, EMA, into the YOLOv8s backbone network [25]. The EMA extracts roller features from the complex background and processes key information to improve conveyor belt deviation detection.

The EMA utilizes a cross-space learning approach by grouping feature maps along channel dimensions into multiple sub-features, ensuring that spatial features are uniformly distributed within each feature group [26]. This design enables the EMA to more effectively

utilize spatial semantic information. Unlike traditional attention mechanisms, which reduce the computational amount through dimensionality reduction, the EMA encodes global information in parallel branches to recalibrate attention weights for each channel, thereby improving the capability of GES-YOLO to extract multi-scale features. Its structure is shown in Figure 3.

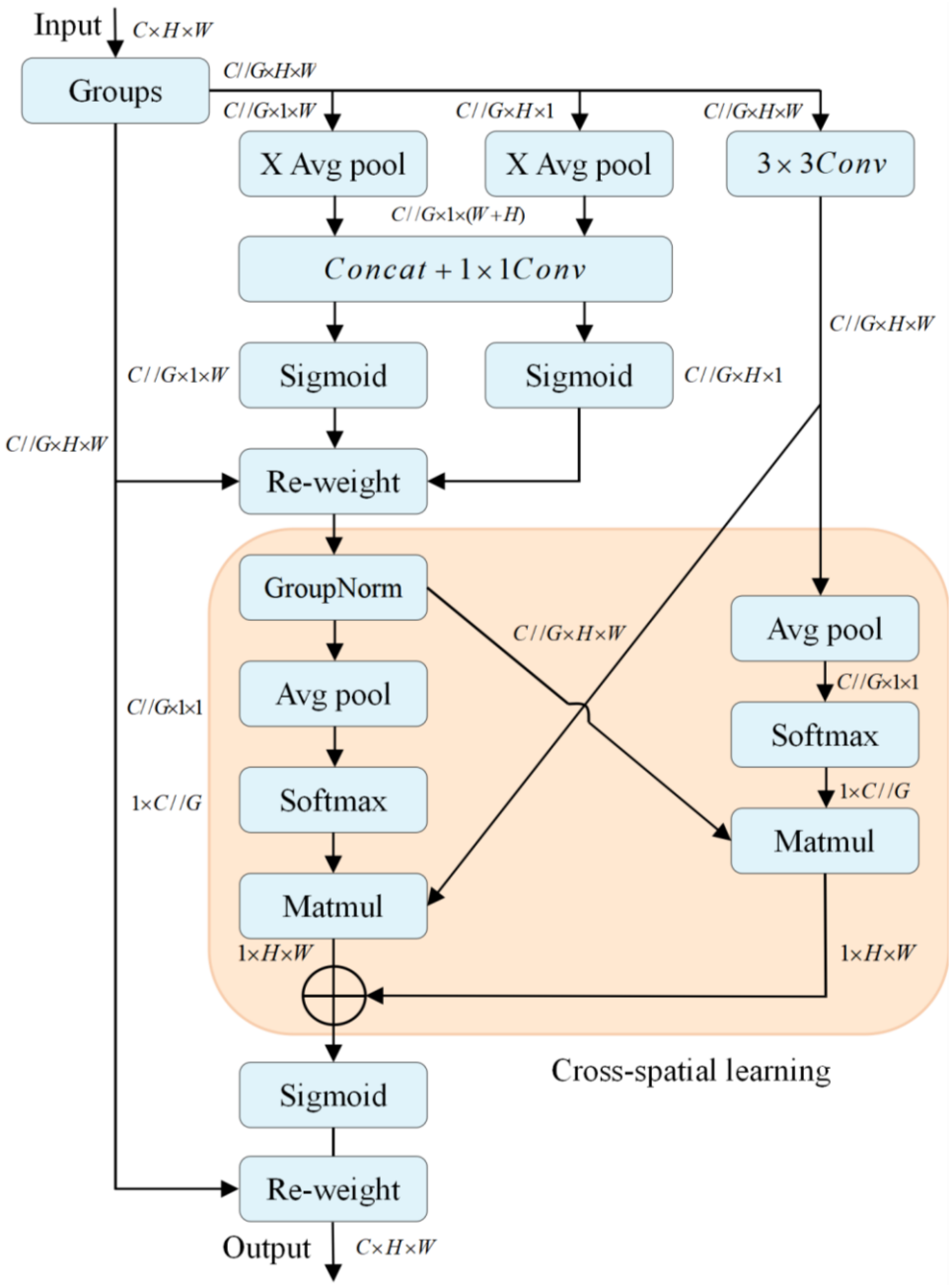


Figure 3. Structure of the EMA.

As depicted in Figure 3, for a given input feature map $X \in R^{C\times H\times W}$, the EMA partitions X into G sub-feature groups along a cross-channel dimension to capture disparate semantic information. Each group's style is denoted as $X = [X_0, X_1, \cdots, X_{G-1}]$, $X_i \in R^{C//G\times H\times W}$. Learned attention weights enhance the representation of important regions in each sub-group. For every sub-feature group, we adopted three parallel paths for extracting attention weights: two 1×1 convolutional branches and one 3×3 convolutional branch. A 1×1 convolutional branch uses adaptive global average pooling operations along both the horizontal and vertical directions. The outputs of the two branches are subsequently

cascaded and aggregated using a shared 1×1 convolution, followed by nonlinear fitting through activation layers. The third branch captures multi-scale feature representations via a single 3×3 convolution. In the cross-space learning component, the 1×1 and 3×3 convolutional branches' outputs are encoded by globally averaging the pooled outputs. The attention weights from different branches are then fused using matrix multiplication. This process effectively aggregates spatial information across different scales to generate the final feature representation.

The introduced EMA improves the ability of GES-YOLO to identify object features, improving its precision in acquiring an object's feature information in the image. It reduces the impact of interference factors and facilitates efficient convolution and extraction of roller feature information from the belt conveyor and, accordingly, improves the detection precision of our model.

2.3. Improve Bounding Box Loss Function

The YOLOv8s model employs the Complete Intersection over Union (CIoU) loss function to compute the bounding box regression loss, with the following definition:

$$L_{CIoU} = 1 - L_{IoU} + \frac{\rho(b, b^{gt})}{c^2} + \alpha\nu \tag{4}$$

where L_{CIoU} represents the value of the loss function, L_{IoU} represents the Intersection over Union (IoU) of the overlapping area between the predicted and ground truth bounding boxes, b refers to the predicted bounding box, b^{gt} indicates the center of the ground truth bounding box, $\rho(\cdot)$ denotes the Euclidean Distance, c^2 denotes the diagonal distance of the minimum enclosing bounding box for the predicted and ground truth boxes, and α and ν are penalty factors. α and ν are calculated using the following equations:

$$\alpha = \frac{\nu}{(1 - L_{IoU}) + \nu} \tag{5}$$

$$\nu = \frac{4}{\pi^2}(\arctan\frac{w^{gt}}{h^{gt}} - \arctan\frac{w}{h})^2 \tag{6}$$

where w represents the width of the predicted bounding box, h represents the height of the predicted bounding box, w^{gt} represents the width of the ground truth bounding box, and h^{gt} represents the height of the ground truth bounding box.

In bounding box regression, the CIoU loss function takes the aspect ratio, centroid distance, and overlap area into consideration, but it does not directly account for the actual aspect ratio between the predicted and ground truth bounding boxes [27]. Such a limitation can hinder optimization of the model and reduce its generalization ability and detection precision. Given the high precision and speed requirements of conveyor belt deviation detection, the SIoU is employed to replace the CIoU loss function in the YOLOv8 network model. The schematic of SIoU loss function computation is presented in Figure 4.

The SIoU loss function is calculated as follows:

$$Loss_{SIoU} = 1 - IoU + \frac{\Delta + \Omega}{2} \tag{7}$$

where IoU denotes the Intersection over Union (IoU) loss, and Δ and Ω represent the distance and shape losses in the loss function, respectively. Their equations are as follows:

$$\Delta = \sum_{t=x,y} (1 - e^{-\gamma\rho_t}) = 2 - e^{-\gamma\rho_x} - e^{-\gamma\rho_y} \tag{8}$$

$$\Omega = (1 - e^{-\omega_w})^{\theta} + (1 - e^{-\omega_h})^{\theta} \tag{9}$$

where $\gamma = 2 - \Lambda$, Λ represents the angle loss, ρ_x is the square of the ratio between C_x and C_w, ρ_y is the square of the ratio between C_y and C_h, ω_w is the ratio of the absolute width difference between the predicted and ground truth bounding boxes to their maximum width, ω_h is the ratio of the absolute height difference between the predicted and ground truth bounding boxes to their maximum height, and θ is the weight coefficient of the shape loss.

The angular loss is defined by the following equation:

$$\Lambda = 1 - 2 \cdot \sin^2(\arcsin(\frac{C_x}{\sigma}) - \frac{\pi}{4}) \tag{10}$$

$$\frac{C_x}{\sigma} = \sin \alpha \tag{11}$$

where σ represents the distance between the center points of the predicted and ground truth bounding boxes, and C_x represents the height difference between the midpoints of the predicted and ground truth bounding boxes.

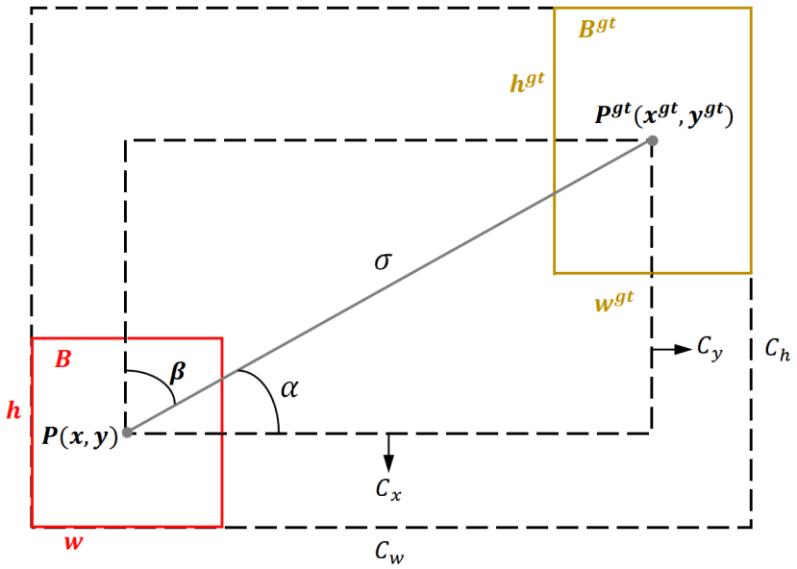


Figure 4. Schematic of the SIoU loss function calculation.

The introduction of the SIoU loss function also takes into account the vector angle between the predicted and ground truth bounding boxes [28]. In comparison with the original CIoU loss function in YOLOv8s, the SIoU loss function incorporates the angle factor, improving the alignment between the predicted and ground truth bounding boxes. This enhances object localization precision while accelerating model convergence.

2.4. Removal of Large Object Detection Layer

In conveyor belt deviation detection, the objects are small, fixed-size rollers. Additionally, the inspection robot that is used for image acquisition is deployed on a track at the top of the coal mine tunnel, which is farther from the conveyor belt, causing the rollers to appear smaller. An analysis of the constructed conveyor belt deviation dataset revealed that 63.4% of the objects in the training set were small (less than 32 × 32 pixels), while only 1.17% were large objects (greater than 96 × 96 pixels). Based on this analysis, we removed the large object detection layer from the YOLOv8s model by eliminating the last two layers of the feature extraction module, preserving feature maps of medium (40 × 40) and small (80 × 80) object detection layers. The feature fusion stage was adjusted according to changes in the backbone network, removing the fusion module for the large object

detection layer in the feature extraction stage. Finally, the large object detection head was removed, retaining only the small and medium object detection headers, further reducing model parameters and improving the computational speed.

3. Experiments and Discussion

3.1. Image Collection and Dataset Construction

The data in this work were collected from monitoring videos of the underground belt conveyor operation at the Yinhe Coal Mine in Shaanxi Province. Frames were extracted at 0.2 s intervals, resulting in a total of 7490 images. After data cleaning, 5975 images with clear objects and distinct features were selected to build the deviation detection dataset for the underground belt conveyor in the coal mine. We classified the dataset into a training set, validation set, and test set in a 7:2:1 ratio. Rollers on left and right sides of belt conveyor were labeled using LabelImg 1.8.0, marked as "roller". The labeling information, including the bounding box coordinates and image category, was recorded to generate the required txt file. The training set consists of 4180 images and 29,277 labels, incorporating various lighting conditions, coal dust, and sample distributions across the images.

3.2. Experimental Environment

The computers that were used for the experiments have the following configurations: AMD 5600H CPU @ 3.30 GHz (Advanced Micro Devices, Santa Clara, CA, USA), 16 GB RAM, NVIDIA GeForce RTX 3050 Ti graphics card (NVIDIA, Santa Clara, CA, USA), Python 3.8.19, PyTorch 1.12.1, and CUDA 11.6. Relevant parameters in the model configuration file were optimized before training to obtain the optimal model. The input image size was 640 × 640, the batch size was 16, the initial learning rate (Lr0) was 0.01, and the training iteration number was 500. While training, a stochastic gradient descent (SGD) optimizer was utilized to optimize our model (momentum = 0.937; weight decay rate = 0.0005).

3.3. Evaluation Indicators

In this paper, the detection precision and speed were used to assess the improved model's performance. The definitions of precision and recall are as follows:

$$Precision = \frac{TP}{TP + FP} \tag{12}$$

$$Recall = \frac{TP}{TP + FN} \tag{13}$$

Precision and *recall* alone cannot fully evaluate the overall performance of the model. Instead, the *F*1-*Score* metric integrates both precision and recall, providing a comprehensive assessment of model performance, which is expressed as follows:

$$F1\text{-}Score = \frac{2TP}{2TP + FN + FP} = \frac{2 \times Precision \times Recall}{Precision + Recall} \tag{14}$$

The area that is enclosed by the two curves (*PR* curve) and the coordinate axes represents the average precision (*AP*), which can be expressed as follows:

$$AP = \int_0^1 P(R)dR \tag{15}$$

The mean precision is calculated on a per-class basis, treating each class independently. To adopt a consistent metric for evaluating the detection performance across all classes, the mean average precision (*mAP*) is used and is defined as follows:

$$mAP = \frac{1}{|n_c|}\sum_{i=1}^{n_c} AP(i) \tag{16}$$

where *TP* represents the number of correctly predicted positive samples, *FP* represents the number of incorrectly predicted positive samples, and *FN* represents the number of incorrectly predicted negative samples. n_c denotes total number of categories.

The *precision* reflects the model's ability to make correct predictions for a given class, *recall* represents the frequency with which the model successfully identifies a specific category, and the *F*1-*Score* is the harmonic mean of the *precision* and *recall* [29]. The average detection precision comprises two metrics: mAP@0.5 and mAP@0.5:0.95. Varying confidence thresholds generate different PR curves. mAP@0.5 indicates a mean accuracy per category at the 0.5 confidence threshold, and mAP@0.5:0.95 indicates a mean accuracy calculated by weighting confidence thresholds between 0.5 and 0.95 in increments of 0.05.

The detection speed is defined as the image number that the model processes within a second, commonly referred to as FPS (Frames Per Second). In object detection tasks, FPS measures the ability of a model to detect and identify objects for as many images as possible within a second. A higher FPS means that the model processes images and generates detection results more quickly, resulting in a higher detection speed.

A network model's complicacy is assessed based on the number of parameters (in M) and floating-point operations (FLOPs, in G). The number of parameters represents the total learnable parameters that are required by the model. Generally, a higher number of parameters corresponds to a more complex model. An increased number of parameters may impose a greater computational burden on training and inference. FLOPs denote the total floating-point operations that are performed during model inference. A higher number of FLOPs indicates a greater computing complicacy, requiring more resources to process images or data.

Based on the above, these metrics enable the evaluation of detection precision, speed, and complexity, allowing us to choose a model that is suited to a specific task and computational resources.

3.4. Experimental Results Using Different Loss Functions

To assess the effects of different loss functions on the model, YOLOv8s is used as the benchmark, and the Distance Intersection over Union (DIoU), Enhanced Intersection over Union (EIoU), Generalized Intersection over Union (GIoU), and SIoU are compared. The experimental outcomes are presented in Table 1. The comparison of the loss curves and mAP@0.5 curves for different loss functions is shown in Figure 5. As shown in Table 1, the SIoU loss function outperforms the other loss functions in the comparative experiments. In comparison with the original CIoU loss function, the SIoU loss function improves the precision from 94.62% to 96.54%, recall from 94.37% to 94.53%, mAP@0.5 from 97.23% to 98.42%, and mAP@0.5:0.95 from 85.49% to 87.44%. The numbers of layers and parameters, 225 and 11.14 M, respectively, remain unchanged.

As shown in Figure 5a, the SIoU loss function exhibits less fluctuation, decreases in loss more rapidly, and achieves a smaller convergence loss in comparison with the CIOU, DIoU, EIoU, and GIoU. Figure 5b shows that the SIoU loss function has a higher mAP value. In summary, the SIoU loss function demonstrates the best convergence, with faster speed and higher localization precision. Therefore, the SIoU loss function is selected as the loss function for the improved model.

Table 1. Comparison of experimental results using different loss functions.

Loss	Precision (%)	Recall (%)	mAP@0.5 (%)	mAP@0.5:0.95 (%)
CIoU	94.62 ± 0.91 SD	94.37 ± 0.79 SD	97.23 ± 0.24 SD	85.49 ± 0.47 SD
DIoU	93.64 ± 1.50 SD	94.42 ± 1.19 SD	97.55 ± 0.34 SD	86.71 ± 0.77 SD
EIoU	91.31 ± 1.99 SD	95.92 ± 1.91 SD	97.91 ± 0.19 SD	86.72 ± 0.43 SD
GIoU	93.32 ± 1.26 SD	94.80 ± 1.12 SD	97.93 ± 0.24 SD	87.02 ± 0.42 SD
SIoU	96.54 ± 1.26 SD	94.53 ± 1.12 SD	98.42 ± 0.15 SD	87.44 ± 0.36 SD

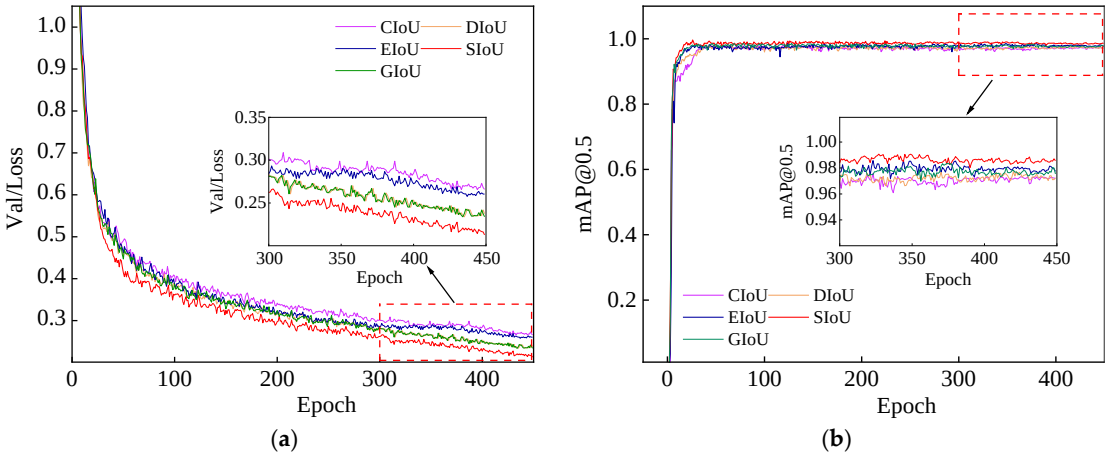


Figure 5. Training results using different loss functions. (**a**) Comparison of loss curves; (**b**) Comparison of mAP@0.5 curves.

To assess the impact of different distance calculation methods on model performance, the YOLOv8s model incorporating the SIoU loss function was used as the baseline model. The model performance was evaluated using four distance calculation methods: Euclidean Distance [30], Manhattan Distance [31], Standardized Euclidean Distance [32], Cosine Distance [33], and Mahalanobis Distance [34]. The experimental results comparing these methods are presented in Table 2.

Table 2. Comparison of experimental results for different distance calculation methods.

Distance	Precision (%)	Recall (%)	mAP@0.5 (%)	mAP@0.5:0.95 (%)
Euclidean Distance	96.54 ± 1.26 SD	94.53 ± 1.12 SD	98.42 ± 0.15 SD	87.44 ± 0.36 SD
Manhattan Distance	95.41 ± 1.79 SD	91.72 ± 1.56 SD	97.25 ± 0.32 SD	85.14 ± 0.59 SD
Standardized Euclidean Distance	92.48 ± 1.37 SD	93.62 ± 1.22 SD	97.76 ± 0.24 SD	86.32 ± 0.51 SD
Cosine Distance	95.87 ± 1.63 SD	91.43 ± 1.39 SD	96.87 ± 0.33 SD	84.26 ± 0.56 SD
Mahalanobis Distance	95.97 ± 1.32 SD	93.84 ± 1.17 SD	97.84 ± 0.16 SD	86.93 ± 0.42 SD

As shown in Table 2, the Euclidean Distance calculation method demonstrated superior performance compared to the other distance calculation methods in the comparaitve experiment. The model using the Euclidean Distance calculation method achieved a precision of 96.54% and a recall of 94.53%, with the highest mAP@0.5 and mAP@0.5:0.95 values of 98.42% and 87.44%, respectively. Additionally, the standard deviations of the four evaluation metrics were the smallest, indicating that this method can maintain a stable detection performance and exhibits good robustness. Therefore, the Euclidean Distance calculation method is selected.

3.5. Results of the Add Attention Mechanism Experiment

This paper improves the ability of GES-YOLO to focus on object features and improves the detection precision by incorporating the Efficient Multi-Scale Attention Mechanism, EMA, after the two C2f modules at the end of the backbone network, leveraging its cross-spatial learning method and multi-scale parallel sub-network. To verify the performance of the EMA attention mechanism, we used the YOLOv8s model with the SIoU loss function as the benchmark and incorporated four attention mechanisms—Shifted Spatial Attention (S2Attention), Squeeze-and-Excitation Attention (SEAttention), Shuffle Attention, and Similarity Attention Mechanism (SimAM)—at the same position in the model's backbone for comparison. The experimental outcomes are shown in Table 3. The test outcomes show that the EMA attention mechanism achieves the highest mAP@0.5 (98.54%) and mAP@0.5:0.95 (86.63%) values, while maintaining fewer parameters and layers. Thus, GES-YOLO is optimized by adding the EMA attention mechanism.

Table 3. Comparison of results from trials using different attention mechanisms.

Attention	Params (M)	FLOPs (G)	Layer	mAP@0.5 (%)	mAP@0.5:0.95 (%)
S2Attention	13.30	30.50	233	97.72 ± 0.20 SD	86.74 ± 0.66 SD
SEAttention	11.23	28.90	232	97.76 ± 0.19 SD	85.17 ± 0.61 SD
Shuffle Attention	11.20	28.90	229	97.62 ± 0.34 SD	86.42 ± 0.74 SD
SimAM	11.20	28.90	227	96.91 ± 0.29 SD	84.33 ± 0.59 SD
EMA	10.81	29.10	223	98.54 ± 0.21 SD	86.63 ± 0.50 SD

3.6. Ablation Experiment

To further improve the detection performance of the YOLOv8s model in the complex conditions of coal mines, this paper adopts four improvement strategies: the GSConv convolution module, the EMA attention module, the SIoU loss function, and the removal of the large object detection layer. To verify the effectiveness of each strategy, ablation experiments were conducted to analyze their impact on the detection performance of the YOLOv8 model. The results are shown in Table 4. The experiments used two different IoU thresholds for mAP, along with the number of parameters (Params) and floating-point operations (FLOPs), as performance evaluation metrics.

The results in the table show that replacing the two Conv modules at the end of the backbone network with the light-weight GSConv module improves the mAP@0.5 and mAP@0.5:0.95 metrics by 0.3% and 0.2%, respectively, in comparison with the YOLOv8s baseline model. Additionally, the number of parameters is reduced by 6.6%, and the computing complicacy decreases by 0.9G, improving object detection precision while achieving a lighter network. This is because the GSConv module performs feature aggregation through both group and spatial convolution, using less time to obtain richer node representations, thus reducing the model complexity and parameters while maintaining detection precision.

The EMA attention mechanism is introduced into the YOLOv8s baseline model to enhance the network's feature extraction capability. The EMA attention mechanism establishes dependencies through multi-scale parallel sub-networks and aggregates information across spatial dimensions by interacting with cross-channel information, effectively fusing cross-spatial and multi-scale features to enhance the detection precision. The results show that introducing the EMA attention mechanism improves the model's mAP@0.5 and mAP@0.5:0.95 by 0.6% and 0.7%, respectively, while reducing the number of parameters by 3.0%.

The SIoU loss function introduces the vector angle between the predicted and ground truth bounding boxes, fully considering their directional relationship. The mAP@0.5 and mAP@0.5:0.95 metrics improve by 1.2% and 2.2%, respectively, without altering the number of model parameters or computing complicacy, enhancing the regression precision.

Table 4. Comparison of ablation experimental results (data in parentheses are the relative rate of change in each parameter relative to the baseline).

GSConv	EMA	SIOU	Drophead	mAP@0.5 (%)	mAP@0.5:0.95 (%)	Params (M)	FLOPs (G)
				97.23 ± 0.24 SD	85.49 ± 0.47 SD	11.14	28.61
√				97.51 ± 0.30 SD (+0.3%)	85.70 ± 0.56 SD (+0.2%)	10.41 (−6.6%)	27.74 (−3.1%)
	√			97.82 ± 0.28 SD (+0.6%)	86.11 ± 0.54 SD (+0.7%)	10.81 (−3.0%)	29.10 (+1.7%)
		√		98.42 ± 0.21 SD (+1.2%)	87.44 ± 0.36 SD (+2.2%)	11.14 (0)	28.61 (0)
			√	96.93 ± 0.24 SD (−0.3%)	85.51 ± 0.72 SD (0)	7.57 (−32.0%)	25.94 (−9.4%)
√	√	√		98.61 ± 0.41 SD (+1.4%)	86.31 ± 0.57 SD (+0.9%)	10.08 (−9.5%)	28.13 (−1.8%)
√		√	√	97.94 ± 0.15 SD (+0.7%)	86.10 ± 0.32 SD (+0.7%)	6.84 (−38.6%)	25.02 (−12.6%)
	√	√	√	98.22 ± 0.15 SD (+1.0%)	86.11 ± 0.42 SD (+0.6%)	7.62 (−31.6%)	26.53 (−7.3%)
√	√	√	√	98.74 ± 0.19 SD (+1.5%)	87.53 ± 0.29 SD (+2.3%)	6.89 (−38.2%)	25.61 (−10.5%)

Further analysis of the experimental outcomes shows that the improvement strategy of removing the large object detection layer reduces the number of parameters and computing complicacy by 32.0% and 9.4%, respectively, at the cost of a 0.3% decrease in the model mAP@0.5 metric. This is because the detection object for conveyor belt deviation consists solely of small rollers, so removing the large object detection layer maintains the detection precision while significantly reducing the number of model parameters and computing complicacy. This small cost results in a significant improvement in model performance.

Finally, all four improvement strategies were integrated into the YOLOv8s baseline model. The results indicate that the proposed GES-YOLO improves mAP@0.5 by 1.5% and mAP@0.5:0.95 by 2.3%, reduces the model parameters by 38.2%, and decreases the computing complicacy by 10.5% in comparison with YOLOv8s. In summary, the GES-YOLO demonstrates higher detection precision for conveyor belt deviation detection in comparison with the YOLOv8s baseline model, with fewer parameters and lower computational requirements. The experimental outcomes confirm the effectiveness and feasibility of the proposed improvement strategy.

3.7. Comparative Experiment

To further validate the practical effectiveness of the GES-YOLO, widely used and industry-representative network models, including the YOLOv5 series, YOLOv8 series, YOLOv9, and YOLOv10, were selected for comparative testing. All models were trained and tested on the same dataset, using identical evaluation metrics as criteria. The experimental outcomes are presented in Table 5.

Based on experimental outcomes, the GES-YOLO proposed in this paper demonstrates significant advantages over other models, except YOLOv5s and YOLOv8n, in key performance metrics such as precision, recall, mAP, number of parameters, computing complicacy, FPS, and model size. While YOLOv8n excels in terms of the number of parameters, computing complicacy, FPS, and model size, its precision is significantly lower than that of the GES-YOLO. Similarly, although YOLOv5s has a slight advantage in computational cost, it lags far behind the GES-YOLO in all other aspects. In contrast, YOLOv5m achieves strong precision but suffers from high model and computing complicacy, making it less suitable for real-time applications. The baseline model shows better performance in precision and FPS

but demonstrates only average results in other metrics. However, in practical applications under harsh environments, these metrics significantly impact detection tasks. Compared with other typical algorithms, the proposed GES-YOLO combines the parameter efficiency of light-weight models with lower computing complicacy, while achieving high precision, recall, mAP, and FPS. Figure 6 presents the comparison of the performances of different models. Therefore, GES-YOLO demonstrates superior precision and outstanding performance in detecting conveyor belt deviation under the complex conditions of underground coal mines. GES-YOLO effectively equilibrates the detection precision and speed, achieving notable results.

Table 5. Comparison of results from the comparative experiment.

Model	Precision (%)	Recall (%)	F1-Score	mAP@0.5 (%)	mAP@0.5:0.95 (%)	Params (M)	FLOPs (G)	FPS	Model Size (MB)
YOLOv5s	90.92 ± 1.97 SD	93.31 ± 1.31 SD	0.92	97.44 ± 0.63 SD	83.21 ± 0.77 SD	7.06	16.54	48.31	13.7
YOLOv5m	93.04 ± 1.13 SD	94.74 ± 0.97 SD	0.94	97.72 ± 0.31 SD	84.01 ± 0.49 SD	21.06	50.62	49.02	40.4
YOLOv8n	91.50 ± 0.94 SD	93.81 ± 1.03 SD	0.93	97.12 ± 0.27 SD	84.24 ± 0.65 SD	3.01	8.20	19.88	5.9
YOLOv8s	94.62 ± 0.91 SD	94.37 ± 0.79 SD	0.94	97.23 ± 0.24 SD	85.49 ± 0.47 SD	11.14	28.61	53.47	22.5
YOLOv9s	93.74 ± 0.99 SD	94.21 ± 1.06 SD	0.94	97.66 ± 0.18 SD	87.23 ± 0.36 SD	7.29	27.44	19.57	14.5
YOLOv10s	93.04 ± 1.53 SD	92.11 ± 1.23 SD	0.93	97.01 ± 0.22 SD	85.32 ± 0.52 SD	8.07	24.83	41.15	15.7
YOLOv11s	95.51 ± 1.03 SD	92.32 ± 0.86 SD	0.94	97.81 ± 0.25 SD	86.82 ± 0.47 SD	9.43	21.51	39.06	19.2
GES-YOLO	96.74 ± 0.97 SD	94.93 ± 0.88 SD	0.96	98.74 ± 0.19 SD	87.53 ± 0.29 SD	6.89	25.61	63.62	13.3

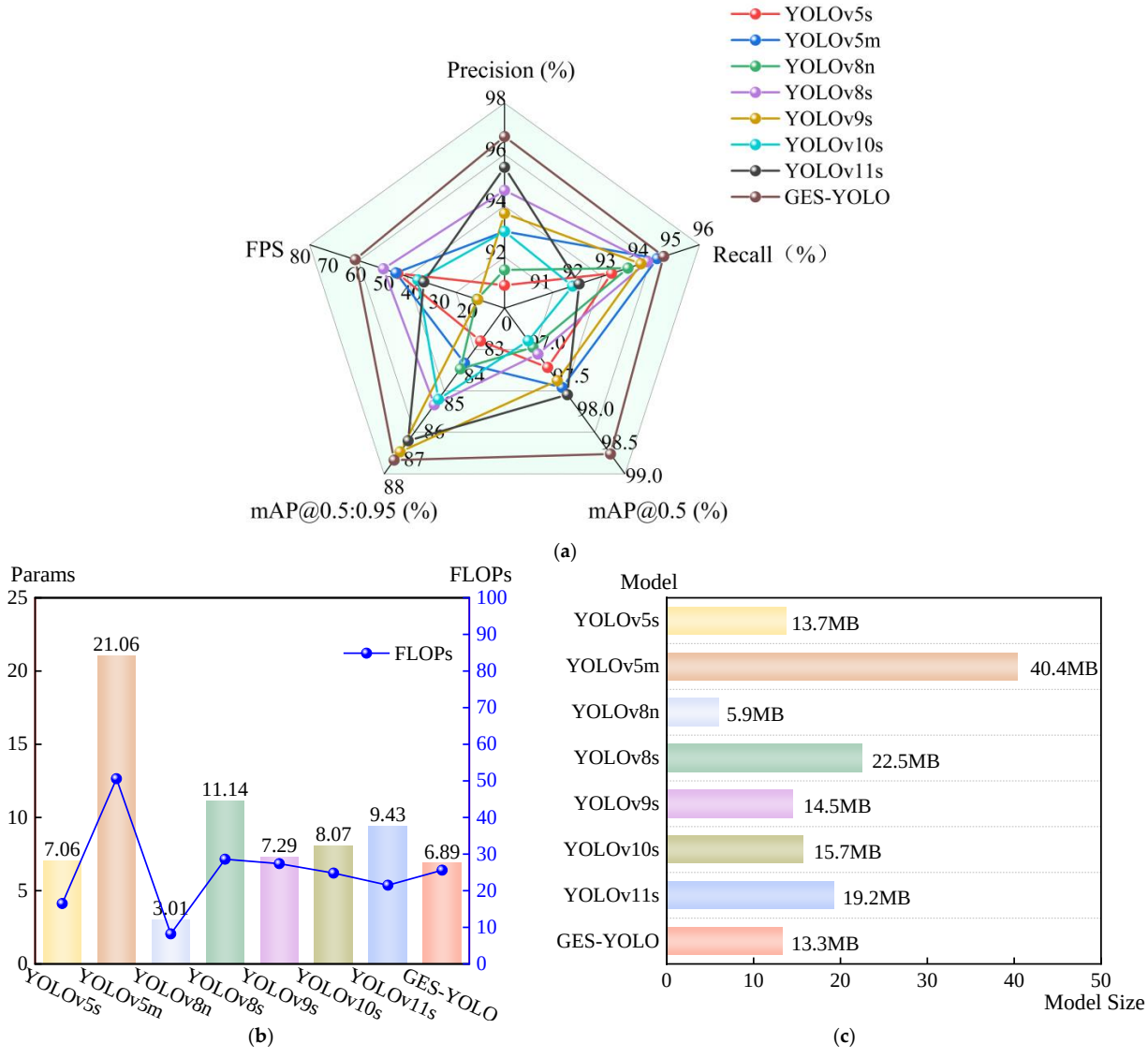


Figure 6. Plot of performance comparison results for different models. (**a**) Performance parameter radar chart; (**b**) params and FLOP results; (**c**) model size results.

3.8. Comparison of Experimental Results

To further evaluate the improved model's performance in real-world applications, video datasets of belt conveyor operations from three coal mines were collected using an inspection robot's remote control platform, and comparative experiments were performed against the YOLOv8s baseline model. The experimental outcomes are illustrated in Figure 7. Figure 7a demonstrates that the baseline model exhibits detection failures caused by coal dust interference and low-light conditions. Figure 7c shows that the baseline model fails to detect belt conveyor rollers at greater distances. GES-YOLO successfully detects rollers at longer distances. Moreover, compared to the YOLOv8s baseline model, the GES-YOLO is capable of identifying and locating the conveyor rollers with higher confidence. It is less affected by factors such as coal dust and lighting and can accurately identify the rollers with stable performance, demonstrating superior robustness.



(**a**) (**b**) (**c**)

Figure 7. Comparison of experimental results: (**a**) First group; (**b**) Second group; (**c**) Third group.

The comparative experimental results fully validate the detection performance of the proposed GES-YOLO model in the complex underground coal mine environment and confirm its effectiveness in practical application scenarios. Figure 8 illustrates the detection performance of the GES-YOLO model based on the belt conveyor operation monitoring video from Yinhe Coal Mine. As shown in the figure, the GES-YOLO model accurately identifies belt conveyor rollers, calculates their distance to the conveyor belt edge, and determines misalignment based on a predefined threshold, ensuring safe and efficient mining operations.

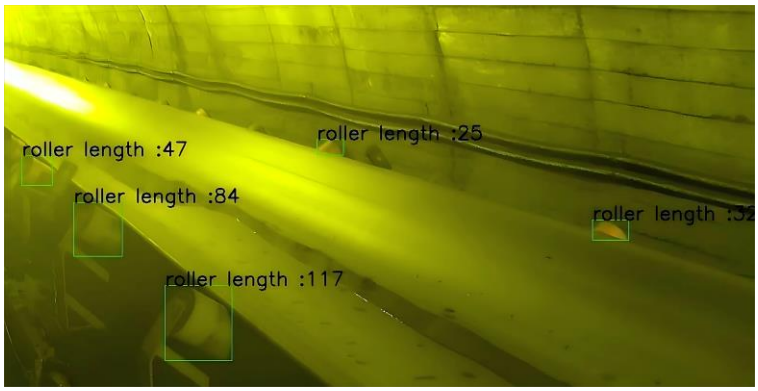


Figure 8. GES-YOLO model conveyor belt deviation detection.

4. Conclusions

To enhance the performance of conveyor belt deviation detection and achieve real-time, high-precision detection under complex operating conditions, this paper proposes a conveyor belt deviation detection algorithm, GES-YOLO, based on an improved YOLOv8s model. The algorithm incorporates four improvement strategies: replacing the Conv modules with light-weight GSConv modules, adding the EMA attention mechanism, using the SIoU loss function instead of the CIoU loss function in the original network, and removing the large object detection layer. These modifications effectively improve the detection accuracy while reducing the computational complexity. The experimental results demonstrate that, compared to the original YOLOv8s model, GES-YOLO achieves a 1.5% and 2.3% increase in mAP@0.5 and mAP@0.5:0.95, respectively. Additionally, the model's parameter count and computational load are reduced by 38.2% and 10.5%, respectively, while the average detection speed reaches 63.62 FPS. Compared to other algorithms, GES-YOLO exhibits the best overall performance and is more suitable for deployment and implementation on edge devices. More importantly, this method provides an economical, efficient, and accurate solution for conveyor belt deviation detection, maintaining excellent performance even in challenging environments such as ones with coal dust and poor lighting. By implementing this method on edge devices, the detection latency can be significantly reduced, enabling timely responses and minimizing conveyor downtime, thereby improving the production efficiency of mines.

In the future, we will address the limitations of the current work by covering conveyor belt deviation detection under different operating environments by continuing to enrich the dataset and conducting model testing and optimization in various mining environments. Additionally, considering that the motion vibrations of inspection robots may impact the detection accuracy in practical applications, future research will focus on mitigating the effects of vibration blur and further optimizing state-of-the-art detection methods.

Author Contributions: Conceptualization, H.W. and Z.K.; methodology, H.W.; software, H.W.; validation, H.W.; formal analysis, H.W. and Y.W.; investigation, H.W.; data curation, H.W.; writing—original draft preparation, H.W.; writing—review and editing, H.W. and Y.W.; project administration, Z.K.; funding acquisition, Z.K. All authors have read and agreed to the published version of the manuscript.

Funding: This research was funded by the following projects: National Natural Science Foundation project (52174147); Research on underground complex working condition detection robot based on domestic Longxin control (key research and development plan project in Shanxi Province); Shanxi Province Mining Equipment Artificial Intelligence and Robotics Technology Innovation Leading Talent Team Project (Project Number: 202204051002003); Research and industrialization of key technologies of intelligent downward feeding telescopic belt conveyor equipment (Mount Taishan Industrial Leading Talent Plan); The research and development of an unmanned management system for belt conveyors based on multiple perception technology, as well as the "unveiling and commanding" project for key core technology research in Taiyuan City; and the Key Technology Research on Intelligent Collaborative Control of Coal Mine Belt Conveyor, Key R&D Program Project of Shanxi Province, 202202150401017.

Data Availability Statement: The data presented in this study are available on request from the corresponding author. The data are not publicly available due to privacy reasons.

Acknowledgments: The authors extend their appreciation to the anonymous reviewers for their valuable feedback.

Conflicts of Interest: The authors declare no conflicts of interest.

References

1. Bai, G.X.; Xu, T.L. Coal Mine Safety Evaluation Based on Machine Learning: A BP Neural Network Model. *Comput. Intell. Neurosci.* **2022**, *2022*, 5233845. [CrossRef] [PubMed]
2. Guo, X.Q.; Liu, X.H.; Zhou, H.; Stanislawski, R.; Królczyk, G.; Li, Z.X. Belt Tear Detection for Coal Mining Conveyors. *Micromachines* **2022**, *13*, 449. [CrossRef] [PubMed]
3. Ji, J.H.; Miao, C.Y.; Li, X.G.; Liu, Y. Speed regulation strategy and algorithm for the variable-belt-speed energy-saving control of a belt conveyor based on the material flow rate. *PLoS ONE* **2021**, *16*, e0247279. [CrossRef]
4. Huang, K.F.; Li, S.Y.; Cai, F.; Zhou, R.H. Detection of Large Foreign Objects on Coal Mine Belt Conveyor Based on Improved. *Processes* **2023**, *11*, 2469. [CrossRef]
5. Wu, X.F.; Wang, C.S.; Tian, Z.Z.; Huang, X.K.; Wang, Q. Research on Belt Deviation Fault Detection Technology of Belt Conveyors Based on Machine Vision. *Machines* **2023**, *11*, 1039. [CrossRef]
6. Wen, L.; Liang, B.; Zhang, L.Y.; Hao, B.N.; Yang, Z.F. Research on Coal Volume Detection and Energy-Saving Optimization Intelligent Control Method of Belt Conveyor Based on Laser and Binocular Visual Fusion. *IEEE Access* **2024**, *12*, 75238–75248. [CrossRef]
7. Zhou, P.; Sun, L.; Zhou, G.B.; Ma, T.B.; Wang, H.R.; Bi, W.Y.; Ma, G.Q.; Wang, W.; Yan, X.D. A New Embedded Condition Monitoring Node for the Idler Roller of Belt Conveyor. *IEEE Sens. J.* **2024**, *24*, 10335–10346. [CrossRef]
8. Wu, L.; Li, J.X.; Zhang, H.Y.; Zhang, W.; Huang, S. Research on a system for the diagnosis and localization of conveyor belt deviations in belt conveyors. *Meas. Sci. Technol.* **2024**, *35*, 035110. [CrossRef]
9. Zhang, M.C.; Shi, H.; Yu, Y.; Zhou, M.S. A Computer Vision Based Conveyor Deviation Detection System. *Appl. Sci.* **2020**, *10*, 2402. [CrossRef]
10. Liu, Y.; Miao, C.Y.; Li, X.G.; Xu, G.W. Research on Deviation Detection of Belt Conveyor Based on Inspection Robot and Deep Learning. *Complexity* **2021**, *2021*, 3734560. [CrossRef]
11. Yang, Y.L.; Miao, C.Y.; Li, X.G.; Mei, X.Z. On-Line conveyor belts inspection based on machine vision. *Optik* **2014**, *125*, 5803–5807. [CrossRef]
12. Zhang, X.; Yang, Z.; Zhang, M.; Yu, Y.; Zhou, M.; Zhang, Y. Quantitative Monitoring Method for Conveyor Belt Deviation Status Based on Attention Guidance. *Appl. Sci.* **2024**, *14*, 6916. [CrossRef]
13. Gao, M.Z.; Li, S.H.; Chen, X.S.; Wang, Y.J. A novel combined method for conveyor belt deviation discrimination under complex operational scenarios. *Eng. Appl. Artif. Intell.* **2024**, *137*, 109145. [CrossRef]
14. Zeng, C.; Zheng, J.; Li, J. Real-Time conveyor belt deviation detection algorithm based on multi-scale feature fusion network. *Algorithms* **2019**, *12*, 205. [CrossRef]
15. Alharbi, F.; Luo, S.H.; Zhang, H.Y.; Shaukat, K.; Yang, G.; Wheeler, C.A.; Chen, Z.Y. A Brief Review of Acoustic and Vibration Signal-Based Fault Detection for Belt Conveyor Idlers Using Machine Learning Models. *Sensors* **2023**, *23*, 1902. [CrossRef]
16. Beck, M.; Maier, G.; Flitter, M.; Gruna, R.; Längle, T.; Heizmann, M.; Beyerer, J. An Extended Modular Processing Pipeline for Event-Based Vision in Automatic Visual Inspection. *Sensors* **2021**, *21*, 6143. [CrossRef]
17. Chen, Y.M.; Sun, X.; Xu, L.; Ma, S.C.; Li, J.; Pang, Y.S.; Cheng, G. Application of YOLOv4 Algorithm for Foreign Object Detection on a Belt Conveyor in a Low-Illumination Environment. *Sensors* **2022**, *22*, 6851. [CrossRef]
18. Rahman, S.; Rony, J.H.; Uddin, J.; Samad, M.A. Real-Time Obstacle Detection with YOLOv8 in a WSN Using UAV Aerial Photography. *J. Imaging* **2023**, *9*, 216. [CrossRef]
19. Siami, M.; Barszcz, T.; Wodecki, J.; Zimroz, R. Automated Identification of Overheated Belt Conveyor Idlers in Thermal Images with Complex Backgrounds Using Binary Classification with CNN. *Sensors* **2022**, *22*, 10004. [CrossRef]
20. Li, S.; Tao, T.; Zhang, Y.; Li, M.; Qu, H. YOLO v7-CS: A YOLO v7-Based Model for Lightweight Bayberry Target Detection Count. *Agronomy* **2023**, *13*, 2952. [CrossRef]
21. Pei, Y.J.; Hou, M.Y.; Han, Q.; Weng, T.F.; Tian, Y.; Chen, G.R.; Liu, J.Y.; Wu, C. ILCS: An Improved Lightweight Convolution Structure and Mixed Interactive Attention for Steel Surface Defect Classification. *Comput. Intell. Neurosci.* **2022**, *2022*, 7539857. [CrossRef] [PubMed]
22. Hulin, L.; Jun, L.; Hanbing, W.; Zheng, L.; Zhenfei, Z.; Qiliang, R. Slim-Neck by GSConv: A lightweight-design for real-time detector architectures. *J. Real Time Image Process.* **2024**, *21*, 62.
23. Gao, M.; Wang, W.; Mao, J.; Xiong, J.; Wang, Z.; Wu, B. QYOLO: Contextual Query-Assisted Object Detection in High-Resolution Images. *Information* **2024**, *15*, 563. [CrossRef]
24. Hao, S.; Ren, K.; Li, J.; Ma, X. Transmission Line Defect Target-Detection Method Based on GR-YOLOv8. *Sensors* **2024**, *24*, 6838. [CrossRef]
25. Zhang, X.D.; Cui, B.; Wang, Z.X.; Zeng, W.T. Loader Bucket Working Angle Identification Method Based on YOLOv5s and EMA Attention Mechanism. *IEEE Access* **2024**, *12*, 105488–105496. [CrossRef]
26. Cao, B.Y.; Jiang, A.S.; Shen, J.C.; Liu, J. Research on Rapid Recognition of Moving Small Targets by Robotic Arms Based on Attention Mechanisms. *Appl. Sci.* **2024**, *14*, 3975. [CrossRef]

27. Zhang, X.R.; Wang, Y.L.; Fang, H.S. Steel surface defect detection algorithm based on ESI-YOLOv8. *Mater. Res. Express* **2024**, *11*, 056509. [CrossRef]
28. Zhang, H.; Shao, F.; He, X.; Chu, W.; Zhao, D.; Zhang, Z.; Bi, S. ATS-YOLOv7: A Real-Time Multi-Scale Object Detection Method for UAV Aerial Images Based on Improved YOLOv7. *Electronics* **2023**, *12*, 4886. [CrossRef]
29. Li, Z.; Li, J.; Zhang, C.; Dong, H. Lightweight Detection of Train Underframe Bolts Based on SFCA-YOLOv8s. *Machines* **2024**, *12*, 714. [CrossRef]
30. Xiong, C.Q.; Zayed, T.; Jiang, X.Y.; Alfalah, G.; Abelkader, E.M. A Novel Model for Instance Segmentation and Quantification of Bridge Surface Cracks-The YOLOv8-AFPN-MPD-IoU. *Sensors* **2024**, *24*, 4288. [CrossRef]
31. Liu, G.X.; Ma, Y.H.; Wang, N. Rolling Bearing Fault Diagnosis Based on SABO-VMD and WMH-KNN. *Sensors* **2024**, *24*, 5003. [CrossRef] [PubMed]
32. Liu, X.C.; Kan, G.Y.; Ding, L.Q.; He, X.Y.; Liu, R.H.; Liang, K. Improving the Performance of Hydrological Model Parameter Uncertainty Analysis Using a Constrained Multi-Objective Intelligent Optimization Algorithm. *Water* **2023**, *15*, 2700. [CrossRef]
33. Pocevice, G.; Stefanovic, P.; Ramanauskaite, S.; Pavlov, E. Approach for Tattoo Detection and Identification Based on YOLOv5 and Similarity Distance. *Appl. Sci.* **2024**, *14*, 5576. [CrossRef]
34. Dashdondov, K.; Lee, S.H.Y.; Erdenebat, M.U. Enhancing Diabetes Prediction and Prevention through Mahalanobis Distance and Machine Learning Integration. *Appl. Sci.* **2024**, *14*, 7480. [CrossRef]

Disclaimer/Publisher's Note: The statements, opinions and data contained in all publications are solely those of the individual author(s) and contributor(s) and not of MDPI and/or the editor(s). MDPI and/or the editor(s) disclaim responsibility for any injury to people or property resulting from any ideas, methods, instructions or products referred to in the content.